

Supporting Information for

**Photochemical Reduction of Nanocrystalline Maghemite to Magnetite**

Hankyeol Jung<sup>a</sup> and Alina M. Schimpf<sup>ab\*</sup>

<sup>a</sup>Materials Science and Engineering Program, <sup>b</sup>Department of Chemistry and Biochemistry  
University of California, San Diego, La Jolla, CA 92093, USA

\*Electronic address: [aschimpf@ucsd.edu](mailto:aschimpf@ucsd.edu)

<b>Supplementary Figures and Tables</b> .....	<b>S2</b>
<b>Figure S1.</b> Full powder X-ray diffraction patterns before and after UV irradiation .....	S2
<b>Table S1.</b> Comparison of $2\theta$ values before and after UV irradiation .....	S2
<b>Table S2.</b> Comparison of unit-cell size for $\gamma$ -Fe <sub>2</sub> O <sub>3</sub> and Fe <sub>3</sub> O <sub>4</sub> .....	S2
<b>Figure S2.</b> Statistical analysis of TEM images before and after UV irradiation .....	S3
<b>Figure S3.</b> Absorption spectra and X-ray diffraction patterns of $\langle d \rangle = 9$ nm nanocrystals ...	S4
<b>Figure S4.</b> Raman spectra of $\langle d \rangle = 9$ nm nanocrystals.....	S5
<b>Figure S5.</b> Titration and heating of photoreduced nanocrystals with Cu(OTf) <sub>2</sub> .....	S6
<b>Figure S6.</b> Titration of photoreduced nanocrystals with (NH <sub>4</sub> ) <sub>2</sub> Ce(NO <sub>3</sub> ) <sub>6</sub> .....	S6
<b>Figure S7.</b> Comparison of extinction spectra of titrated and as-synthesized nanocrystals .....	S7
<b>Table S3.</b> Summary of titration results .....	S7
<b>Table S4.</b> Comparison of ensemble photoreduction rates .....	S7
<b>Figure S8.</b> Photoreduction in the presence of added acetaldehyde .....	S8
<b>Figure S9.</b> Extinction spectra of nanocrystals (photo)reduced with LiEt <sub>3</sub> BH.....	S8
<b>Figure S10.</b> Powder X-ray diffraction pattern after UV irradiation with LiEt <sub>3</sub> BH .....	S9
<b>Table S5.</b> Exchange bias before and after UV irradiation .....	S10
<b>Figure S11.</b> Magnetism of $\langle d \rangle = 9$ nm nanocrystals before and after UV irradiation .....	S10
<b>Figure S12.</b> Powder X-ray diffraction pattern of photoreduced $\langle d \rangle = 9$ nm nanocrystals ...	S11
<b>Figure S13.</b> Comparison of photoreduction of $\gamma$ -Fe <sub>2</sub> O <sub>3</sub> and $\gamma$ -Fe <sub>2</sub> O <sub>3</sub> /Fe <sub>3</sub> O <sub>4</sub> nanocrystals ....	S11
<b>Experimental Methods</b> .....	<b>S12</b>
<i>Chemicals</i> .....	S12
<b>Table S6.</b> Chemicals .....	S12
<i>Nanocrystal synthesis</i> .....	S12
<b>Table S7.</b> Preparation of anaerobic solutions for optical measurements .....	S13
<i>Elemental analysis</i> .....	S13
<i>Photoreduction for optical measurements</i> .....	S13
<i>Titrations</i> .....	S13
<i>Photoreduction in the presence of acetaldehyde</i> .....	S13
<i>Powder X-ray diffraction</i> .....	S14
<i>Transmission electron microscopy</i> .....	S14
<i>Raman spectroscopy</i> .....	S14
<i>Magnetometry</i> .....	S15
<b>References</b> .....	<b>S15</b>

## Supplementary Figures and Tables

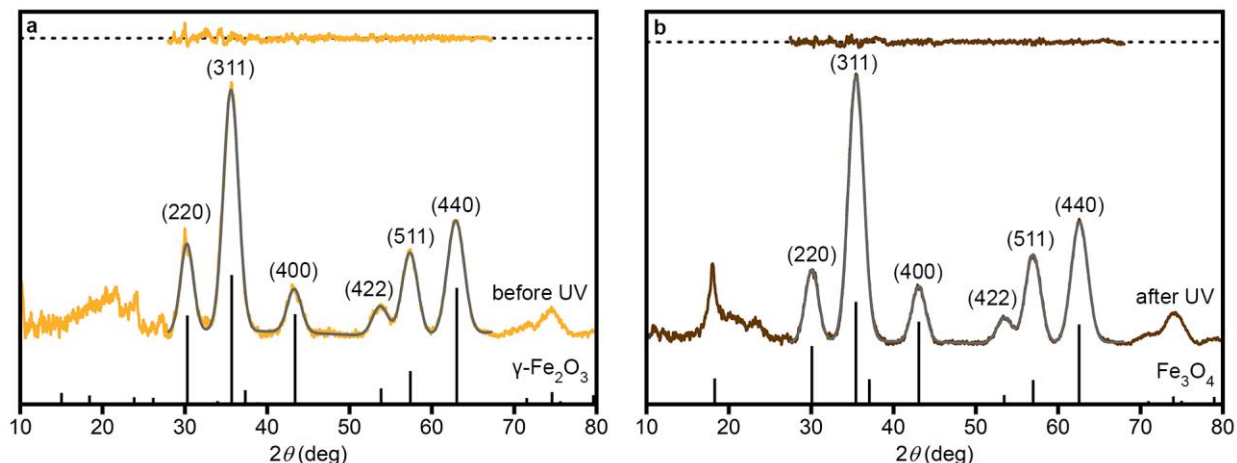


**Figure S1.** Full powder X-ray diffraction patterns of  $\langle d \rangle = 4.8$  nm nanocrystals (a) before and (b) after UV irradiation. Experimental patterns are compared to those simulated from single-crystal data for  $\gamma\text{-Fe}_2\text{O}_3$  (250541, ref. 1) and  $\text{Fe}_3\text{O}_4$  (ICSD# 26410, ref. 2), respectively. Experimental patterns were fit from  $2\theta \approx 28\text{--}67^\circ$  (gray trace) and the residuals shown for comparison (top). These fits were used to evaluate the changes upon photoreduction (Table S1). All patterns are plotted for diffraction of Cu  $K\alpha$  radiation ( $1.5406 \text{ \AA}$ ).

**Table S1.** Comparison of  $2\theta$  values for representative reflections of  $\langle d \rangle = 4.8$  nm nanocrystals before (oxidized) and after (photoreduced) UV irradiation with EtOH or  $\text{LiEt}_3\text{BH}$ . Experimental values are derived from fits to the powder patterns (Figure S1). Values for  $\gamma\text{-Fe}_2\text{O}_3$  (ICSD# 250541, ref. 1) and  $\text{Fe}_3\text{O}_4$  (ICSD# 26410, ref. 2) simulated from single-crystal data are given for comparison. All values are given for diffraction of Cu  $K\alpha$  radiation ( $1.5406 \text{ \AA}$ ).

Reflection (hkl)	$\gamma\text{-Fe}_2\text{O}_3$ (ref. 1)	Oxidized	Photoreduced with EtOH	$\text{Fe}_3\text{O}_4$ (ref. 2)
220	30.301	$30.249 \pm 0.004$	$30.082 \pm 0.002$	30.087
311	35.692	$35.600 \pm 0.001$	$35.459 \pm 0.001$	35.439
400	43.383	$43.288 \pm 0.008$	$43.066 \pm 0.003$	43.070
422	53.831	$53.731 \pm 0.013$	$53.479 \pm 0.008$	53.431
511	57.388	$57.327 \pm 0.005$	$56.944 \pm 0.002$	56.958
440	63.028	$62.899 \pm 0.003$	$62.595 \pm 0.002$	62.545

**Table S2.** Comparison of unit-cell size for  $\gamma\text{-Fe}_2\text{O}_3$  and  $\text{Fe}_3\text{O}_4$ .

	$a$ ( $\text{\AA}$ )	ICSD #	Ref.
$\gamma\text{-Fe}_2\text{O}_3$	8.3364	250541	1
$\text{Fe}_3\text{O}_4$	8.3941	26410	2

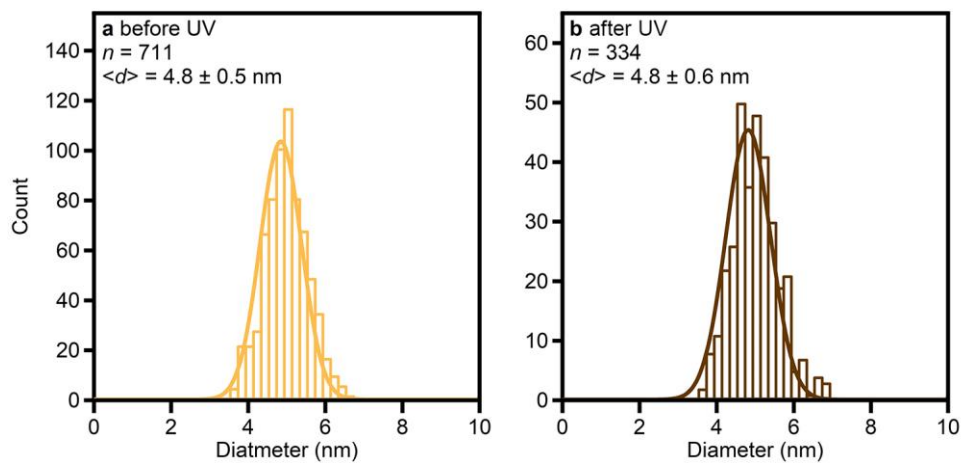


**Figure S2.** Statistical analysis of TEM images of  $\langle d \rangle = 4.8 \text{ nm}$   $\gamma\text{-Fe}_2\text{O}_3$  nanocrystals **(a)** before and **(b)** after 3 h UV irradiation in the presence of EtOH.

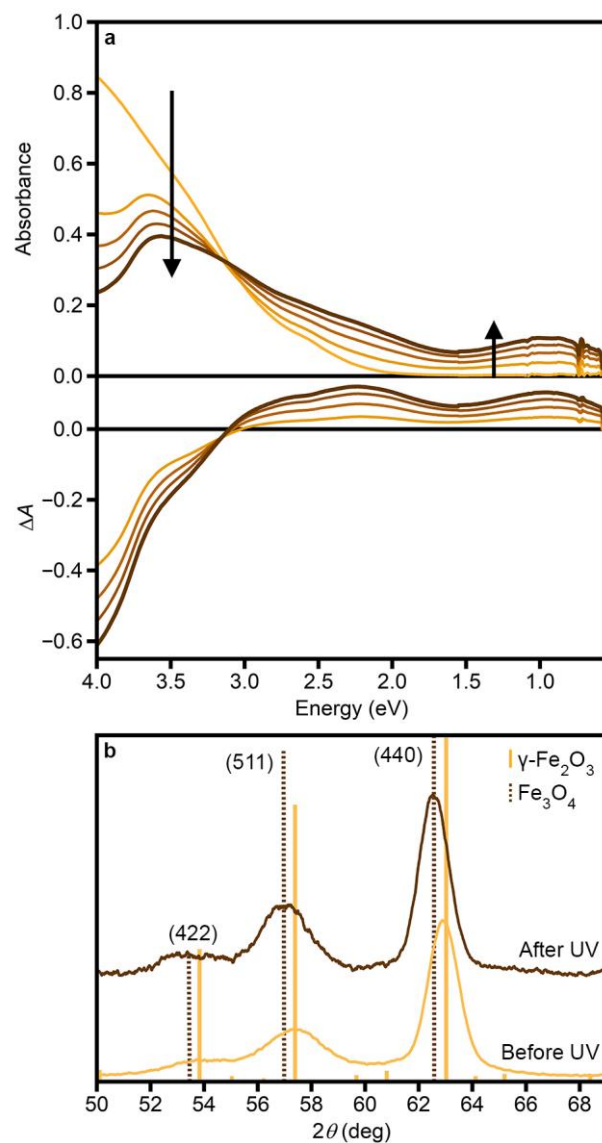


**Figure S3.** Photochemical conversion of  $\gamma\text{-Fe}_2\text{O}_3$  to  $\text{Fe}_3\text{O}_4$  in  $\langle d \rangle = 9.0$  nm nanocrystals. **(a)** Absorption spectra of nanocrystals ( $[\text{Fe}] = 0.98$  mM) with increasing UV-irradiation time. **(b)** Powder X-ray diffraction patterns before (yellow) and after (brown) 48 h UV irradiation. Simulated patterns for  $\gamma\text{-Fe}_2\text{O}_3$  (solid yellow)<sup>1</sup> and  $\text{Fe}_3\text{O}_4$  (dashed brown)<sup>2</sup> are shown for reference. All patterns are plotted for diffraction of Cu K $\alpha$  radiation (1.5406 Å).

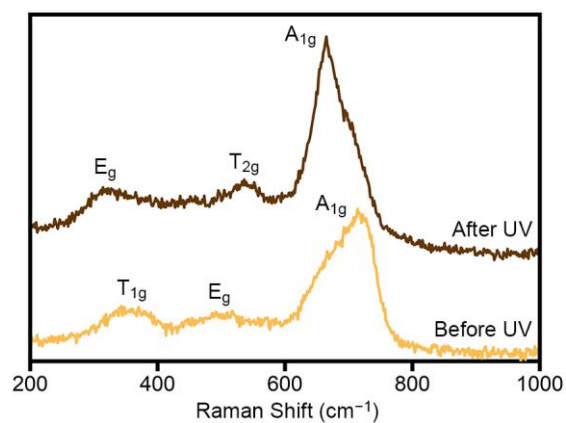


**Figure S4.** Raman spectra of  $\langle d \rangle = 9.0$  nm nanocrystals before (yellow) and after (brown) 40 h UV irradiation. Peak assignments, including the narrowing and blueshifting of the A<sub>1g</sub> mode upon UV irradiation, are indicative of conversion to magnetite.<sup>3-4</sup>

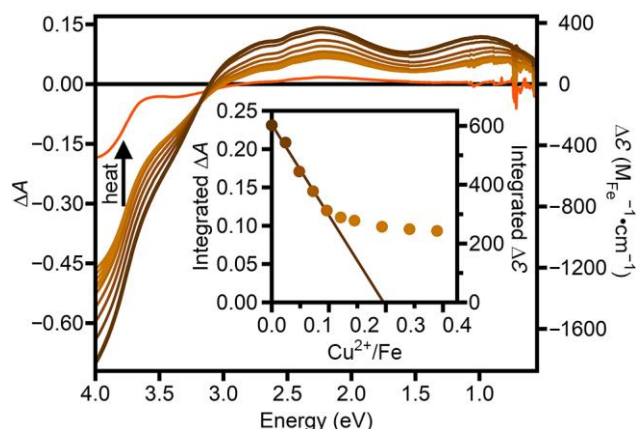


**Figure S5.** Absorption and extinction (plotted as  $\Delta A = A - A_{\text{BeforeUV}}$  and  $\Delta \varepsilon = \varepsilon - \varepsilon_{\text{BeforeUV}}$ , respectively) spectra of photoreduced  $\langle d \rangle = 4.8$  nm nanocrystals ( $[\text{Fe}] = 1.0$  mM) with added  $\text{Cu}(\text{OTf})_2$ . Inset: Integrated (0.8–3.0 eV)  $\Delta A$  as a function of  $\text{Cu}^{2+}/\text{Fe}$ . The linear fit is used to estimate the fraction of  $\text{Fe}^{2+}$  in the photoreduced nanocrystals. After 0.18 equiv  $\text{Cu}^{2+}/\text{Fe}$ , further  $\text{Cu}(\text{OTf})_2$  addition leads to very little change in the absorption spectra. The solution of nanocrystals + 0.58 equiv  $\text{Cu}(\text{OTf})_2$  was heated for 2 h at 85 °C to further drive the oxidation.

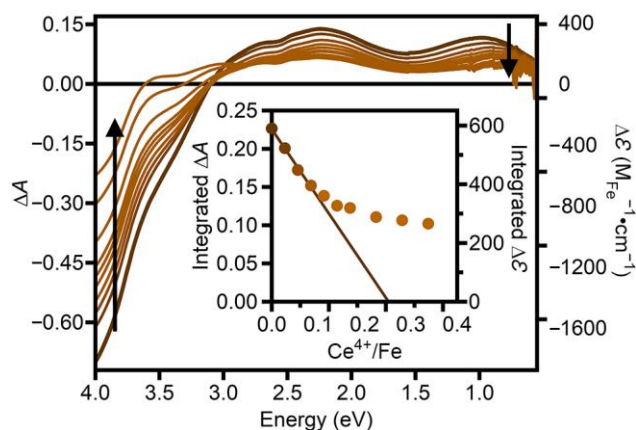


**Figure S6.** Absorption and extinction (plotted as  $\Delta A = A - A_{\text{BeforeUV}}$  and  $\Delta \varepsilon = \varepsilon - \varepsilon_{\text{BeforeUV}}$ , respectively) spectra of photoreduced  $\langle d \rangle = 4.8$  nm nanocrystals ( $[\text{Fe}] = 1.0$  mM) with added  $(\text{NH}_4)_2\text{Ce}(\text{NO}_3)_6$ . Inset: Integrated (0.8–3.0 eV)  $\Delta A$  as a function of  $\text{Ce}^{4+}/\text{Fe}$ . The linear fit is used to estimate the fraction of  $\text{Fe}^{2+}$  in the photoreduced nanocrystals (41 %). After 0.14 equiv  $\text{Ce}^{4+}/\text{Fe}$ , further  $(\text{NH}_4)_2\text{Ce}(\text{NO}_3)_6$  addition leads to relatively little change in the absorption spectra.

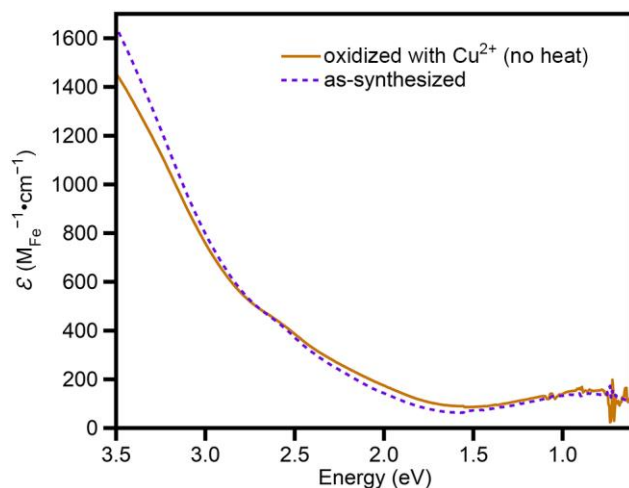


**Figure S7.** Extinction spectra of maximally photoreduced  $\langle d \rangle = 4.8$  nm nanocrystals ( $[\text{Fe}] = 1.0$  mM) with 0.58 equiv  $\text{Cu}(\text{OTf})_2$  per Fe added (solid brown) compared to that of as-synthesized nanocrystals (dashed purple).

**Table S3.** Summary of titration results for  $\langle d \rangle = 4.8$  nm nanocrystals photoreduced with EtOH as the sacrificial reductant.

Oxidant	% $\text{Fe}^{2+}$
$\text{Cu}(\text{OTf})_2$	39 (Figure 2)
$\text{Cu}(\text{OTf})_2$	47
$\text{Cu}(\text{OTf})_2$	45
$(\text{NH}_4)_2\text{Ce}(\text{NO}_3)_6$	41
<b>Average</b>	<b><math>43 \pm 4</math></b>

**Table S4.** Size-dependence of ensemble photochemical reduction rate,  $k$ , determined by fitting the data in Figure 3 (inset) to  $\Delta\mathcal{E} = C(1 - e^{-kt})$ .

$\langle d \rangle$ (nm)	$k$ ( $\text{h}^{-1}$ )
4.8	1.8
7.3	1.1
9.0	0.90

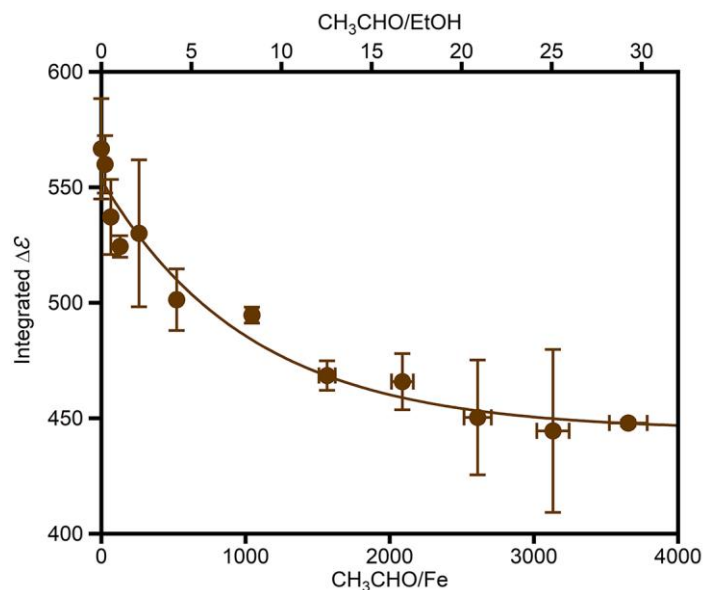


**Figure S8.** Integrated extinction intensities ( $\Delta\varepsilon = \varepsilon - \varepsilon_{\text{BeforeUV}}$ ) for  $\langle d \rangle = 4.8$  nm nanocrystals maximally photoreduced in the presence of added acetaldehyde ( $\text{CH}_3\text{CHO}$ ). The solid line is a guide to the eye.

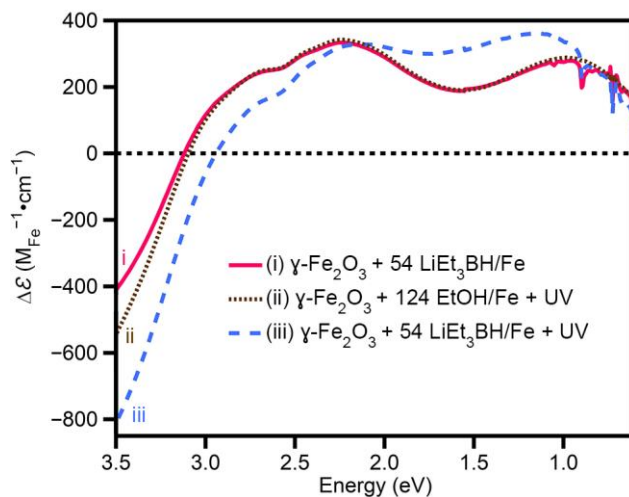


**Figure S9.** (i) Differential extinction spectrum ( $\Delta\varepsilon = \varepsilon - \varepsilon_{\text{NoLiEt}_3\text{BH}}$ ) of  $\langle d \rangle = 4.8$  nm nanocrystals with added  $\text{LiEt}_3\text{BH}$  in the dark compared to (ii) the differential extinction spectrum ( $\Delta\varepsilon = \varepsilon - \varepsilon_{\text{BeforeUV}}$ ) of the same nanocrystals maximally photoreduced with  $\text{EtOH}$ . (iii) UV irradiation of  $\text{LiEt}_3\text{BH}$ -treated nanocrystals leads to further spectroscopic changes.

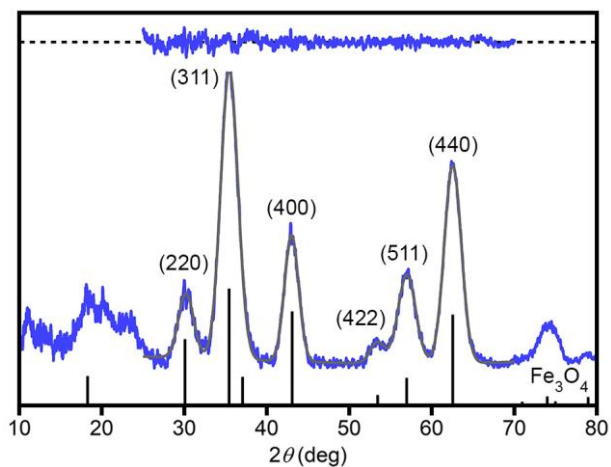


**Figure S10.** Powder X-ray diffraction pattern of  $\langle d \rangle = 4.8$  nm nanocrystals after 5 h UV irradiation in the presence of  $\text{LiEt}_3\text{BH}$ . The pattern for  $\text{Fe}_3\text{O}_4$  simulated from single-crystal data (ICSD# 26410, ref. 2) is shown for comparison. The experimental pattern was fit from  $2\theta \approx 28\text{--}67^\circ$  (gray trace) and the residuals shown for comparison (top). All patterns are plotted for diffraction of Cu  $K\alpha$  radiation ( $1.5406 \text{ \AA}$ ).

**Table S5.** Exchange bias ( $H_E$ ) of iron oxide nanocrystals with varying amounts of UV irradiation

Irradiation time (h)	$H_E$ (Oe)
4.8 nm (Figure 4)	
0	-0.04
1	-0.39
6.5	1.19
9.0 nm (Figure S11)	
0	9.01
1.5	-118
4	-117

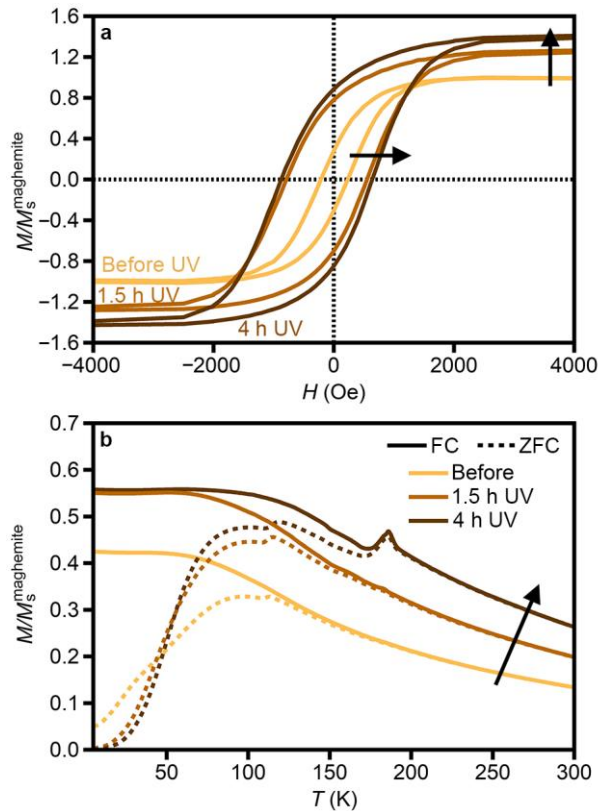


**Figure S11.** Magnetic properties following UV irradiation of  $\langle d \rangle = 9.0$  nm nanocrystals. Magnetization as a function of (a) applied field at 5 K and (b) temperature for field-cooled (FC, solid lines, 100 Oe) and zero-field-cooled (ZFC, dashed lines) samples. All magnetization values ( $M$ ) are given in terms of  $M_s^{\text{maghemite}}$ , which is the saturation magnetization at 5 K of the maghemite nanocrystals before UV irradiation. Arrows show changes with increasing UV irradiation.

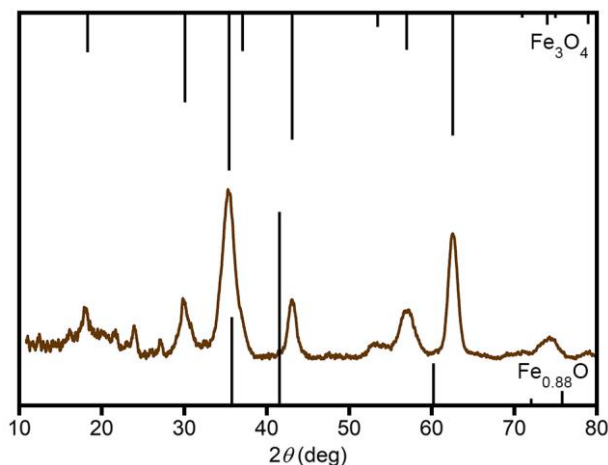


**Figure S12.** Powder X-ray diffraction pattern of  $\langle d \rangle = 9.0$  nm nanocrystals after 48 h UV irradiation with EtOH as a sacrificial reductant. The patterns for  $\text{Fe}_{0.88}\text{O}$  (bottom, ICSD# 67203, ref. <sup>5</sup>) and  $\text{Fe}_3\text{O}_4$  (ICSD# 26410, ref. <sup>2</sup>) simulated from single-crystal data is shown for comparison. All patterns are plotted for diffraction of Cu K $\alpha$  radiation (1.5406 Å).

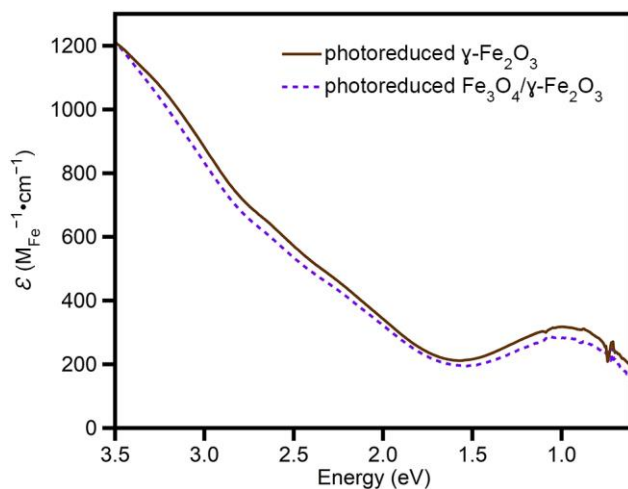


**Figure S13.** Extinction spectra of maximally photoreduced as-synthesized ( $\gamma$ - $\text{Fe}_2\text{O}_3$ / $\text{Fe}_3\text{O}_4$ , dashed purple) and oxidized ( $\gamma$ - $\text{Fe}_2\text{O}_3$ )  $\langle d \rangle = 4.8$  nm nanocrystals with EtOH as the sacrificial reductant

## Experimental Methods

*Chemicals.* Chemical manufacturers and purities are given in Table S6. Toluene (tol) and tetrahydrofuran (THF) were obtained from a solvent purification system, transferred to a nitrogen-filled glovebox and stored over molecular sieves (3 Å) for 24 h prior to use.

**Table S6.** Chemicals

Chemical	Purity	Manufacturer
<i>Chemicals used in <math>\gamma</math>-Fe<sub>2</sub>O<sub>3</sub> nanocrystal synthesis</i>		
Iron pentacarbonyl (Fe(CO) <sub>5</sub> )	99.5%	Strem Chemicals
Oleic acid (OA)	>97%	Aldrich
Diocetyl ether (C <sub>16</sub> H <sub>34</sub> O)	>98%	Aldrich
Dibenzyl ether (C <sub>14</sub> H <sub>14</sub> O)	>95%	Alfa Aesar
<i>Chemicals used for post-synthetic redox experiments</i>		
Anhydrous ethanol (EtOH)	90%	Strem Chemicals
tert-Butyl alcohol (t-BuOH)	99.5%	Alfa Aesar
Lithium triethylborohydride (LiEt <sub>3</sub> BH, 1 M in THF)	1.00 M	Alfa Aesar
Copper(II) trifluoromethanesulfonate (Cu[OTf] <sub>2</sub> )	99.95%	Oakwood
Ammonium cerium (IV) nitrate (CAN)	>98.0%	TCI
Acetaldehyde (CH <sub>3</sub> CHO)	99%	Alfa Aesar
<i>Other chemicals</i>		
Nitric acid (HNO <sub>3</sub> , 69%), TraceMetal grade		Fisher Chemical
Hydrogen peroxide (H <sub>2</sub> O <sub>2</sub> , 31%) for ultratrace analysis		Sigma Aldrich

*Nanocrystal Synthesis.* Colloidal  $\gamma$ -Fe<sub>2</sub>O<sub>3</sub> nanocrystals were prepared by thermal decomposition of iron pentacarbonyl (Fe(CO)<sub>5</sub>) in the presence of oleic acid (OA), adapting a previously published synthesis.<sup>6</sup> In a typical synthesis of nanocrystals with  $\langle d \rangle \approx 5$  nm, 10 ml dibenzyl ether (52.6 mmol) and 1.43 ml OA (4.56 mmol) were degassed in a 100-ml 3-neck round-bottom flask at 100 °C for 2 h. The solution was then placed under a nitrogen atmosphere and 0.2 ml (1.52 mmol) Fe(CO)<sub>5</sub> was rapidly injected. The resulting mixture was heated to reflux (~290 °C) at the rate of 8 °C/min and held for 1 h, after which it was cooled to room-temperature. Nanocrystals with  $\langle d \rangle \approx 7$  nm were obtained using a similar method, with a faster heating rate of 3 °C/min. Nanocrystals with  $\langle d \rangle \approx 9.0$  nm were obtained using a similar method, replacing dibenzyl ether with an equivalent volume of dioctyl ether (33.2 mmol) and heating at 3 °C/min. A quarter of the resulting solution was taken to prepare the as-synthesized stock solution and the remaining nanocrystals were oxidized by heating at 100 °C in air (8–48 h) until the IVCT was not visible by absorption measurements at [Fe] ~ 1 mM.

After cooling the solution to room-temperature, ~0.1 ml OA was added to the solution and the mixture was sonicated for 10 s. The nanocrystals were washed by adding EtOH to the reaction mixture and centrifuging at 15000 rpm for 5 min. The resulting pellets were resuspended in toluene/EtOH (1/3) and centrifuged again at 15000 rpm for 5 min. The addition of toluene/EtOH followed by centrifugation was repeated a total of 3 times. After the third centrifugation, the resulting pellet was dried under vacuum for 2 h on a Schlenk line, after which it was brought into a nitrogen-filled glovebox and resuspended in 10–20 ml anaerobic toluene. As-synthesized and

oxidized nanocrystals were processed following the same procedure. The [Fe] of each stock solution is provided in Table S7.

**Table S7.** Preparation of anaerobic solutions for optical measurements

$\langle d \rangle$ (nm)	[Fe] in anaerobic stock solution (mM)	Volume of stock solution ( $\mu\text{l}$ )	Volume of toluene ( $\mu\text{l}$ )	Volume of THF ( $\mu\text{l}$ )	[Fe] in cuvette (mM)
4.8	21	68	682	750	0.96
7.3	30	50	700	750	1.0
9.0	41	36	714	750	0.98

*Elemental analysis.* 50  $\mu\text{l}$  anaerobic stock solution was dried under vacuum and digested in 2 ml  $\text{HNO}_3/\text{H}_2\text{O}_2$  (1/1) for 1 day.<sup>7</sup> 100  $\mu\text{l}$  of the digested solution was diluted in 9.9 ml ultrapure  $\text{H}_2\text{O}$  with 5%  $\text{HNO}_3$ . 1 ml diluted solution was further diluted in 9 ml ml ultrapure  $\text{H}_2\text{O}$  with 5%  $\text{HNO}_3$ . Inductively coupled plasma–mass spectrometry (ICP–MS) was collected on a Thermo iCAP RQ ICP–MS.

*Photoreduction for optical measurements.* In a typical experiment with  $\langle d \rangle = 4.8$  nm nanocrystals, 68  $\mu\text{l}$  anaerobic stock solution, 682  $\mu\text{l}$  toluene and 750  $\mu\text{l}$  THF were loaded into a 4-mm screw-cap cuvette (final [Fe]  $\sim 1.0$  mM). To this solution, 10  $\mu\text{l}$  EtOH (124 equiv per Fe) was added as a sacrificial reductant. The absorption spectrum of the as-prepared solution was collected using a Cary 5000 spectrometer. The solution was irradiated with a 365-nm LED ( $0.5 \text{ W}/\text{cm}^2$ ) and the absorption spectrum was monitored periodically. Nanocrystals were considered to be maximally photoreduced when no change in the absorption spectrum was observed over 30 min. Under these conditions, maximum photoreduction levels were typically reached within 2, 3, or 5 h for  $\langle d \rangle = 4.8, 7.3$  or 9.0 nm, respectively. For larger nanocrystals, the volume of stock solution was adjusted such that all solutions used for optical measurements had similar [Fe] (Table S7). For photoreduction with  $\text{LiEt}_3\text{BH}$ , 68  $\mu\text{l}$  anaerobic stock solution, 682  $\mu\text{l}$  toluene, and 750  $\mu\text{l}$   $\text{LiEt}_3\text{BH}$  (0.1 M in THF, 54 equiv per Fe) were loaded into a 4-mm screw-cap cuvette. Addition of  $\text{LiEt}_3\text{BH}$  to the nanocrystals resulted in a color-change and absorption measurements revealed reduction prior to UV irradiation.

*Titrations.* The cuvette containing maximally photoreduced  $\langle d \rangle = 4.8$  nm nanocrystals was brought into a nitrogen-filled glovebox. A solution of oxidant (0.014 M) was prepared by dissolving 41.5 mg  $\text{Cu}(\text{OTf})_2$  (0.115 mmol) or 63.0 mg CAN (0.115 mmol) in 8 ml acetonitrile in a nitrogen-filled glovebox. To the cuvette containing maximally photoreduced nanocrystals, 10  $\mu\text{l}$  oxidant solution was added and mixed by vigorous shaking. After each addition, the absorption spectrum was recorded. The addition of oxidant solution was repeated until 90–100  $\mu\text{l}$  was added in total. The integrated intensities (0.8–3.0 eV) of the differential absorption spectra were plotted as a function of oxidant equivalents. The first 5 data points (in which integrated intensity decreased linearly with added oxidant) were fit to a line, where the  $x$ -intercept was the fraction of Fe that had been oxidized (equal to the fraction of  $\text{Fe}^{2+}/\text{Fe}_{\text{total}}$ ). For titrations with mild heating, the cuvette was heated on a hotplate at the lowest setting for 2 h. The temperature was measured using an IR gun to be 85  $^\circ\text{C}$ .

*Photoreduction in the presence of acetaldehyde.* In a typical experiment, 1 ml anaerobic stock solution was diluted with 10 ml toluene. From this diluted solution, 750  $\mu\text{l}$  was loaded into a 4-mm screw-cap cuvette and to it was added 750  $\mu\text{l}$  THF and 10  $\mu\text{l}$  EtOH. This solution was the "0

equiv acetaldehyde" control. When adding acetaldehyde, the volume of THF was adjusted to maintain a constant [Fe] and total volume. Each solution was irradiated with 365-nm LED (0.5 W/cm<sup>2</sup>) and the absorption spectrum was monitored periodically. Nanocrystals were considered to be maximally photoreduced when no change in the absorption spectrum was observed over 30 min.

*Powder X-ray diffraction.* For measurements on oxidized samples, nanocrystals were precipitated by adding with 0.5 ml EtOH to 0.5 ml anaerobic stock solution and collected via centrifugation at 15000 rpm for 5 min. The resulting pellets were dried under vacuum (2 h) and stored under nitrogen for 1 h prior to the measurement. For measurements on photoreduced samples, maximally photoreduced samples (1.5 ml, ~1 mM) were brought into a nitrogen-filled glovebox and precipitated with 0.5 ml EtOH in air-tight centrifuge tubes. Precipitates were collected via centrifugation at 15000 rpm for 5 min and resuspended in toluene (0.5 ml). Precipitation with EtOH followed by centrifugation was repeated a total of 3 times. After the third centrifugation, the resulting pellets were dried under vacuum (2 h) and stored under nitrogen for 1 h prior to the measurement. X-ray diffraction patterns were collected at 300 K using a Bruker Apex II Single-Crystal X-ray Diffractometer equipped with a Mo K $\alpha$  radiation source ( $\lambda = 0.7107\text{\AA}$ ) and Apex II area Detector. The measurement was performed in transmission mode with detector distance of 200 mm and 3 frames collected  $\phi = 0^\circ$  and  $45^\circ$ . The first, second, and third frames were centered at  $2\theta = 10^\circ$ ,  $22^\circ$ , and  $34^\circ$ , respectively. The diffraction rings obtained from the three frames were overlaid together and radially integrated in Diffrac.eva software. Single-crystal corundum (Bruker) was used as a calibration standard. To report the reflection locations, powder patterns were fit in the range of  $2\theta = 26\text{--}68$  deg with a cubic baseline and Gaussian peaks. Fitting was performed using the Wavemetrics Multi-Peak Fitting Package in Igor.

*Transmission electron microscopy.* "Before UV" sample: In a nitrogen-filled glovebox, 0.1 ml anaerobic stock solution was diluted with ~1 ml toluene. The diluted solution was removed from the glovebox and ~20  $\mu\text{l}$  was drop-cast onto a 100-mesh copper TEM grid coated with formvar and carbon (Electron Microscopy Sciences). "After UV" sample: Nanocrystals were maximally photoreduced following the method used for optical measurements. Outside of the glovebox, ~20  $\mu\text{l}$  photoreduced solution was removed from the cuvette and drop-cast onto the TEM grid. Grids were examined using either a JEOL JEM-1400Plus transmission electron microscope operating at 80 kV equipped with a Gatan OneView 4K digital camera ( $\langle d \rangle = 4.8$  nm) or a FEI Spirit microscope operating at 80 kV equipped with a 2k $\times$ 2k Gatan CCD camera ( $\langle d \rangle = 7.3$  nm and 9.0 nm). Images were transformed into contrast-binary image files and sizing and statistical analyses were performed using the "Analyze Particles" function in ImageJ. The resulting data were histogrammed with 0.2-nm bins and fit with a Gaussian distribution.

*Raman spectroscopy.* "Before UV" sample: In a nitrogen-filled glovebox, 0.5 ml anaerobic stock solution was transferred to an air-tight centrifuge tube and mixed with 0.5 ml EtOH to precipitate the nanocrystals. The mixture was centrifuged at 15000 rpm for 5 min. The addition of toluene/EtOH in the glovebox followed by centrifugation was repeated a total of 3 times, after which the resulting pellet was transferred to a Si substrate.

"After UV" sample: In a nitrogen-filled glovebox, 250  $\mu\text{l}$  anaerobic stock solution was transferred to a 4-mm screw-cap cuvette containing 500  $\mu\text{l}$  toluene, 750  $\mu\text{l}$  THF and 100  $\mu\text{l}$  EtOH. The cuvette was irradiated by UV for 40 h. In the glovebox, 0.5 ml photoreduced solution was transferred to an air-tight centrifuge tube and mixed with 0.5 ml EtOH to precipitate the nanocrystals. The addition of toluene/EtOH followed by centrifugation was repeated a total of 3 times, after which the resulting pellet was transferred to a Si substrate. Raman spectra were

collected on freshly prepared samples using a Renishaw inVia confocal Raman microscope with 532-nm laser-excitation (5 mW) and a 50× objective lens.

*Magnetometry.* 750  $\mu\text{l}$  anaerobic stock solution was mixed with 750  $\mu\text{l}$  THF and 10  $\mu\text{l}$  EtOH. From this diluted solution,  $\sim$ 50 mg was loaded into a pre-massed, customized quartz tube. The mass of the loaded solution was recorded by and the tube was then sealed anaerobically using an  $\text{H}_2/\text{O}_2$  torch. Magnetic data was collected on the as-prepared sample ("Before UV"). The quartz tube was then irradiated using a 365-nm LED ( $0.5 \text{ W}/\text{cm}^2$ ) and the magnetization data were collected after various irradiation times. Magnetic data were collected by a Quantum Design MPMS3 SQUID magnetometer. Field-dependent magnetization data ( $M-H$ ) were collected at 5 K (cooled under zero-field) and 300 K and temperature-dependent magnetization data ( $M-T$ ) were collected at 100 Oe.

## References

1. Solano, E.; Frontera, C.; Puig, T.; Obradors, X.; Ricart, S.; Ros, J. Neutron and X-Ray Diffraction Study of Ferrite Nanocrystals Obtained by Microwave-Assisted Growth. A Structural Comparison With the Thermal Synthetic Route. *J. Appl. Crystallogr.* **2014**, *47*, 414.
2. Fleet, M. The Structure of Magnetite. *Acta Crystallogr. B* **1981**, *37*, 917.
3. Testa-Anta, M.; Ramos-Docampo, M. A.; Comesana-Hermo, M.; Rivas-Murias, B.; Salgueirino, V. Raman spectroscopy to unravel the magnetic properties of iron oxide nanocrystals for bio-related applications. *Nanoscale Adv.* **2019**, *1*, 2086.
4. Dar, M. I.; Shivashankar, S. A. Single crystalline magnetite, maghemite, and hematite nanoparticles with rich coercivity. *Rsc Advances* **2014**, *4*, 4105.
5. Radler, M. J.; Cohen, J. B.; Faber, J. Point-Defect Clusters in Wüstite. *J. Phys. Chem. Solids* **1990**, *51*, 217.
6. Hyeon, T.; Lee, S. S.; Park, J.; Chung, Y.; Bin Na, H. Synthesis of Highly Crystalline and Monodisperse Maghemite Nanocrystallites Without a Size-Selection Process. *J. Am. Chem. Soc.* **2001**, *123*, 12798.
7. Gu, L.; Fang, R. H.; Sailor, M. J.; Park, J. H. In Vivo Clearance and Toxicity of Monodisperse Iron Oxide Nanocrystals. *ACS Nano* **2012**, *6*, 4947.